Wave-by-Wave Control of a Wave Energy Converter with Deterministic Wave Prediction

U. A. Korde*, R. D. Robinett, III*, D. G. Wilson†, G. Bacelli† and O. O. Abdelkhalik*
*Mechanical Engineering–Engineering Mechanics, Michigan Technological University
Houghton, MI, USA
E-mail: uakorde@mtu.edu
†Sandia National Laboratories, Albuquerque, NM, USA

***Abstract*—This paper discusses wave-by-wave near-optimal control of a wave energy device in irregular waves. A deterministic propagation model is used to predict the wave elevation several seconds into the future at the device location. Two prediction approaches are considered. The first is based on a time series being measured over an advancing time window at a particular up-wave location. This approach is here utilized in long-crested irregular waves. The second approach uses successive snapshots of wave elevation measurements over an up-wave area. This approach is found more convenient for multi-directional waves, and is here applied in a bi-directional wave irregular wave field. A small, heaving vertical cylinder reacting against a deeply submerged (i.e. assumed to undergo negligible oscillations) mass is studied under wave-by-wave control. The non-causal feedforward control force required for optimum velocity under a swept-volume constraint is based on the past, current, and predicted wave elevation at the device. Results for time-averaged converted power and displacement/force maxima are obtained for a range of irregular wave conditions. Also presented in addition are energy conversion results with a feedback-alone control force using a multi-resonant control technique.**

***Index Terms*—Hydrodynamic modelling, control, wave prediction, deterministic prediction, directional waves**

I. Introduction

Floating bodies oscillating relative to a reference have been used for energy conversion for several decades [1]. Active control of the hydrodynamic response of such bodies provides one way to enhance annual energy conversion with small devices, thereby increasing the likelihood of cost-effective operation (see for instance, [2]). Indeed, efforts to increase response bandwidth by controlling the phase of the force applied by the power take-off were first reported in the seventies [3] and [4]. For the Salter duck, control was accomplished by including a reactive component in addition to the resistive part in the torque opposing the duck oscillation, and by independently adjusting the magnitudes of the two parts. Investigations on small heaving point-absorber devices with short resonant periods led to the development of the 'latching' concept [5]. Work on single-mode reactive control led to multiple-mode impedance matching approaches termed 'complex-conjugate control' ([6], [7], etc), which could be applied in the frequency-domain for peak-frequency tuning in changing wave spectra. At-sea tests on reactive + resistive loading were performed a few years ago on prototypes of the Wave Star device [8], and a 2-3 fold improvement in annual power production was reported.

Latching control has received considerable attention over the last 3 decades (e.g. see [9], [10], [11], [12], [13], [14], etc). The determination of an optimal latching sequence was first addressed under an optimal control framework in [9] with the device dynamic model providing a dynamic constraint. The optimum switching sequence was determined with the help of the Pontryagin Max/Min Principle (often following an iterative approach). A declutching approach was later introduced mainly for devices with longer resonance periods than the prevailing energy periods [15], [16]. Even though the applied forces are purely resistive, evaluation of the switching sequence requires prediction of the wave or exciting force into the future. With either latching or declutching the sudden application or release of large forces/moments can lead to transient vibrations through the entire system, which, in addition to the force/moment load magnitudes, should be considered early in the design process, and could be problematic in some applications.

In contrast, the control considered in this work requires smoothly varying actuation forces/moments. It should be noted that power conversion through a particular oscillation mode is maximized when oscillations occur at the hydrodynamically optimum velocity. In general, as discovered in the tests on the duck, this is not possible without using an external actuator to apply a control force and without exchanging reactive power with the device. Application of reactive and resistive loads to produce correct impedance matching conditions on a wave-by-wave basis in irregular waves presents a fundamental challenge. As has been known since the mid-eighties, wave-by-wave control of a wave energy converter for maximum power conversion requires knowledge or prediction of the incoming wave field [17], [18].

As just pointed out, hydrodynamically optimum velocity requires a non-causal force at each instant, which cannot fully be evaluated without knowledge or prediction of the wave surface elevation information from the future. Naito and Nakamura [17] used the wave profile measured up-wave to generate a control force. Forsberg [19] used an autoregressive-moving average (ARMA) model to predict the incident waves for a real wave record and found a reasonably close match. Belmont [20] discussed deterministic prediction of surface elevations

using two approaches: (i) the fixed-point approach, in which a sufficiently long time series of wave profile measurements at a single point is used, and (ii) the fixed-time approach, where a 'snap shot' of the wave profile over a sufficiently long distance is used in conjunction with a deterministic propagation model. One of the authors of this paper used the fixed-point approach in long-crested (i.e. uni-directional) irregular waves to generate the instantaneous control force for wave-by-wave control of a 2-body axisymmetric wave energy converter [21]. The length of the time-series and the up-wave distance were set based on the required prediction time (i.e. time into the future up to which prediction is needed for a truncated control force impulse response function) and the range of group velocities associated with 'commonly' encountered ocean wave spectra. Root-mean-square errors up to about 7% were observed. The effect of prediction errors on energy conversion was analyzed in [22]. Note that in [21], propagation was assumed to be dispersive, and accounted for all component wave groups spanning the range of group velocities associated with practical wave spectra. For this reason, the incident wave predictions in [21] would be expected to be more accurate than that reported in [20], where the prediction was ultimately obtained using a single group velocity corresponding to the shallow-water limit. Use of up-wave measurements was reported in [23], which also considered use of the autoregressive time-series prediction (see also, [24]). Implicit in the use of up-wave measurements in [23] appears to have been the use of a non-dispersive wave propagation model (i.e. a single, shallow-water velocity). It may be worth investigating whether prediction accuracy would be improved by adding dispersive propagation effects, and further, by more fully accounting for the diffraction and radiation flux dynamics of the oscillating water column chamber. Other workers have considered direct prediction of exciting force over a geometry-dependent prediction time (e.g. [25]), which is a potentially attractive approach, though its extension to multi-mode energy conversion remains to be explored. Such a generalization is relatively straightforward with wave-elevation prediction, since predicted wave elevations are available at chosen points on the device.

This paper presents results for a fixed-time approach, and the prediction accuracy is compared with that using the fixed-point approach. The fixed-time approach is more straightforward to extend to multi-directional waves and hence is examined further for a range of wave-incidence angles varying over a sector. Note, however, that prediction of surface elevations for directional waves within a direction band using fixed-point measurements was considered in [26]. Currently available commercial technology for wave measurements over an area (as opposed to at a point, for which a wave-rider buoy would be sufficient) includes the X-band nautical radar, coupled with the WaMOS software to provide wave statistical information such as significant wave height, energy period, etc. However, recent developments based on WaMOS II also include the ability to predict wave elevations, as demonstrated in a wave basin for assumed directional distributions [27]. Evaluation of multi-directional spectra from X-band measurements was performed in a recent work [28], though surface elevation predictions were not made. Thus, real-sea applications of the present approach could use images acquired by an X-band radar. For the purpose of the present work, the irregular wave records are generated using standard directional spectra. Predictions are compared with exact wave elevations. To illustrate an application of the technique, time-domain simulation results for an oscillation-constrained axi-symmetric heaving device with feedforward control based on bi-directional incident wave prediction are presented. While the present results could be compared with other feedforward based approaches such as model predictive control implementations, the main interest here is in comparing them with with results based on a control technique that uses feedback alone ('multi-resonant control'), together with power electronics circuitry. Note that this control technique does not require wave prediction, since only displacement/velocity feedback is needed for control force evaluation. Calculations are also performed for pure resistive loading (which does not involve real-time feedback or feedforward inputs) with a view to providing a baseline for the feedforward and feedback control approaches.

II. Fixed-Point Measurement for Prediction

The propagation model is understood here as the relationship between the measured wave elevation at some point on the surface some time in the past (and the present), and the predicted wave elevation at a different point in space some time in the future. Wave elevation measurements may be available in the form of time series at fixed points ('fixed-point approach') or 'snapshots' over a fixed area at a single instant ('fixed-time approach'). Typically, distances on the order of 1000m and prediction times in the neighborhood of 30s are adequate in most realistic sea states/spectra [17], [18], and [21]. If the dynamics of wind-wave interactions over the free-surface are ignored over such distance and time scales, a linear kinematic model relating the wave surface elevation $\eta(x;t)$ at one point (time) and the wave surface elevation at another point and another time may be sufficient, though the implied Fourier transformability requires that the wave elevation $\eta(x,t) \to 0$ as $t \to \pm\infty$ [29], [30]. In practice, this would restrict application of the fixed-point approach to periods of wave activity between periods when the sea is relatively calm.

In deep water, for uni-directional wave propagation, a kinematic model relating the wave elevation at point x_A to that at point x_B in the frequency domain can be expressed as

$$\eta(x_B;i\omega) = \mathrm{e}^{-ik(\omega)d}\eta(x_A;i\omega) \tag{1}$$

where $k(\omega)$ using the deep-water dispersion relation is

$$k(\omega) = \frac{|\omega|\omega}{g} \tag{2}$$

$k(\omega)$ has the same sign as ω. The wave elevation time history for predominantly uni-directional waves may be obtained by a non-directional wave rider buoy. For most realistic surface wave spectra over which a wave energy device operates, ω is

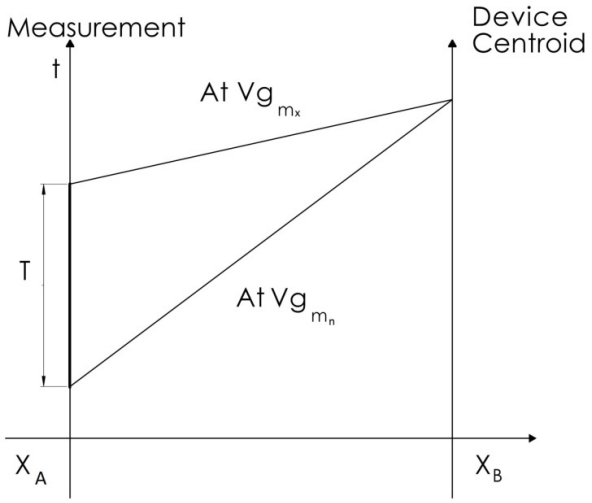

Fig. 1. A space-time diagram showing the relationship between the group velocity range considered, the prediction time into the future, the up-wave distance, and the length of the time series needed.

contained within finite approximate limits ω_l and ω_h. Because surface waves are dispersive, an impulsive excitation of the wave surface propagates over a range of group velocities $[v_{gmn}, v_{gmx}]$, where, for deep water,

$$\begin{aligned} v_{gmn} &= \frac{1}{2}\left(\frac{g}{\omega_{mx}}\right) \\ v_{gmx} &= \frac{1}{2}\left(\frac{g}{\omega_{mn}}\right) \end{aligned} \tag{3}$$

The relationship between the measured time series at x_A and the prediction at x_B at an instant t_p into the future is shown in the space-time diagram of Figure 1. For the fixed-point approach, a prediction at x_B using a measurement at x_A can be obtained using an impulse response function $h_l(t)$ where

$$h_l(t;d) = \frac{1}{2\pi}\int_{-\infty}^{\infty} \mathrm{e}^{-ik(\omega)d}\mathrm{e}^{i\omega t}d\omega \tag{4}$$

$h_l(t)$ can be evaluated analytically as [18], [20], and [21] as

$$\begin{aligned} h_l(t;d) =& \frac{1}{4}\sqrt{\frac{2g}{\pi d}}\left[\cos\left(\frac{gt^2}{4d}\right) + \sin\left(\frac{gt^2}{4d}\right)\right] \\ &+ \frac{1}{2}\sqrt{\frac{2g}{\pi d}}\left[\cos\left(\frac{gt^2}{4d}\right)\mathrm{C}\left(t\sqrt{\frac{g}{2\pi d}}\right)\right] \\ &+ \frac{1}{2}\sqrt{\frac{2g}{\pi d}}\left[\sin\left(\frac{gt^2}{4d}\right)\mathrm{S}\left(t\sqrt{\frac{g}{2\pi d}}\right)\right] \end{aligned} \tag{5}$$

where the Fresnel integrals C and S have been used. Using a wave surface-elevation time-series measurement at x_A over $[t-T, t]$ seconds, the surface elevation at $x_B = x_A + d$ at time $t + t_p$ can be obtained using

$$\begin{aligned} &\eta(x_B; t+t_p) = \int_0^T h_l(\tau)\eta(x_A; t-\tau)d\tau;\ t > T \\ &x_B - x_A = d = t_P v_{gmx} \\ &T = \frac{d}{v_{gmn}} - \frac{d}{v_{gmx}} \end{aligned} \tag{6}$$

Section X discusses one result for this approach [21], which compares the predicted wave elevation with the directly computed wave elevation for an irregular wave record.

III. Errors due to Directionality

It is worthwhile to examine the effect of wave directionality on the accuracy of the uni-directional propagation model of equation (5). Thus, if the actual propagation direction of the incident waves is β, then the distance parameter d should be replaced by $d\cos\beta$, and a prediction at x_B using the h_l in equation (5) will contain an error. An observation of the right side of $h_l(t;d)$ shows that the direction error β will affect both the coefficient on the bracket, and the arguments of both the trigonometric functions and the Fresnel integrals. For instance, a Taylor series expansion of the coefficient $\sqrt{\frac{2g}{\pi d}}$ about $\beta = 0$ shows that the error in h_l varies as β^2. Similarly, the error in the arguments of the trigonometric functions relative to $\beta = 0$ can also be seen to be on the order of β^2. Approximating the combined effect of the coefficient and the argument errors to be on the order of β^2, the root-mean-square error in the predicted wave elevation can be estimated for known errors in measured wave elevations. More details on this calculation are included in [31], where it is argued that the root-mean-square error in the predicted wave elevation is proportional to the root-mean-square error in h_l and for small β, increases as β^2, which would be serious in practical applications.

IV. Prediction in Multi-directional Waves

It is supposed here that incident waves approach the device from a range of angles $[\pi/2, 3\pi/2]$ (see Figure 2). Such may be the case when a device is some distance away from the shoreline, and not at a point in the open ocean where storm surges and wind waves could approach from any direction within the range $[\pi/2, 5\pi/2]$. However, the treatment summarized below could be extended without much difficulty to a wider range of incidence angles as required. Assuming small-amplitude waves as before, the wave surface elevation for a wave front approaching from a direction β at a point (r, θ) on the free surface can be represented as

$$\eta(r, \theta; t) = A\mathrm{e}^{-i(kr\cos(\beta-\theta)-\omega t)} \tag{7}$$

where k is the scalar wave number. The complete wave record at (r, θ) is a linear superposition of waves spanning a range of wave numbers, approaching from a range of directions. Further, k is related to frequency ω via the dispersion relation. It is easy to see that the fixed-point approach has limited utility

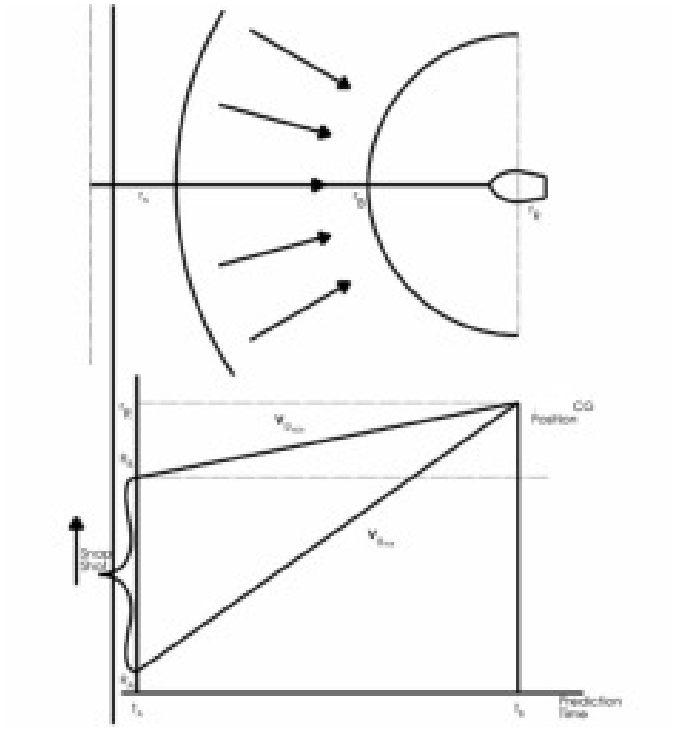

Fig. 2. A space-time diagram for the multi-directional prediction using a snap-shot of wave elevation measurements. Note that distances are now on the vertical axis, with time on the horizontal axis.

in this situation, as, the wave elevation at point (r, θ) is the combined effect of waves of different frequencies approaching from multiple directions, where (r, θ) may be either the point of wave measurement or the point where prediction is required. A single point measurement thus provides insufficient information for prediction. In contrast, a 'snap-shot' measurement over a large enough area at one instant could provide sufficient information for a prediction at a short time into the future and at a chosen point down-wave of the measurement area. Such a measurement could be obtained with an X-band radar, as pointed out in section I. The space-time diagram describing this situation is included in Figure 2.

It is assumed here that wave activity very far from the device has no influence over the spatial scales of interest to the measurement and prediction procedure (so that it can be assumed to be negligible). A convenient initial illustration of the fixed-time approach is provided by the case of uni-directional propagation, where the prediction based on this approach must match that based on the fixed-point measurement case summarized in section II.

Here, as in section II,

$$\eta(x;t) = A\mathrm{e}^{-i(kx-\omega t)} \tag{8}$$

For the fixed-time approach, a 'snap-shot' wave surface elevation is obtained over a spatial domain at time t, and prediction is needed at time $t+p$ at the location of the device. The appropriate impulse response function in this case, for uni-directional propagation is,

$$h_p(d;p) = \frac{1}{2\pi}\int_{-\infty}^{\infty} \mathrm{e}^{-ikd}\mathrm{e}^{i\sqrt{gk}p}dk \tag{9}$$

This impulse response function can be shown to be,

$$\begin{aligned} h_p(d;p) =& \sqrt{\frac{\pi g}{2d}}\frac{p}{d}\left[\cos\left(\frac{gp^2}{4d}\right)\mathrm{C}\left(\sqrt{\frac{g}{d}}\frac{p}{2}\right)\right] \\ &+ \sqrt{\frac{\pi g}{2d}}\frac{p}{d}\left[\sin\left(\frac{gp^2}{4d}\right)\mathrm{S}\left(\sqrt{\frac{g}{d}}\frac{p}{2}\right)\right] \\ &+ \sqrt{\frac{\pi g}{2d}}\frac{p}{d}\left[\cos\left(\frac{gp^2}{4d}\right)+\sin\left(\frac{gp^2}{4d}\right)\right] \end{aligned} \tag{10}$$

This impulse response function provides a prediction p seconds ahead in time and at the location of the device centroid x_B, using a 'snap-shot' wave-elevation measurement at time t over a spatial distance D, where

$$\begin{aligned} D &= v_{gmx}p - v_{gmn}p \\ x_h &= x_o + D \\ x_B &= x_h + v_{gmn}p \end{aligned} \tag{11}$$

Then,

$$\eta(x_B; t+p) = \int_{x_o}^{x_h} h_p(x-\xi)\eta(\xi; t+p)d\xi \tag{12}$$

Note that, in this case, the device centroid is at x_B, and the snap-shot measurement stretches from x_o to x_o+D. x_o may be chosen based on the instrument measurement range providing the snap-shot measurement. A simulation result comparing the prediction obtained using equation (12) with the directly evaluated value at $(x_B; t+p)$ for an irregular wave record is included in section X.

It can be shown that the impulse-response function $h_p(d;p)$ of equation (10) for multi-directional waves now needs to be appended to include angular information and becomes,

$$\begin{aligned} &h_p(d,\theta;p) = \\ &\int_{\pi/2}^{3\pi/2}\sqrt{\frac{\pi g}{2\overline{r}}}\left(\frac{p}{\overline{r}}\right)\cos\left(\frac{gp^2}{4\overline{r}}\right)\left[1+\mathrm{C}\left(\sqrt{\frac{g}{\overline{r}}}\frac{p}{2}\right)\right]d\beta \\ &+\int_{\pi/2}^{3\pi/2}\sqrt{\frac{\pi g}{2\overline{r}}}\left(\frac{p}{\overline{r}}\right)\sin\left(\frac{gp^2}{4\overline{r}}\right)\left[1+\mathrm{S}\left(\sqrt{\frac{g}{\overline{r}}}\frac{p}{2}\right)\right]d\beta \end{aligned} \tag{13}$$

where $\overline{r} = r\cos(\beta-\theta)$. Further, it is more convenient to carry out the integration over β numerically in order to obtain the final form for $h_p(d,\theta;p)$. If the device centroid is located at $(r_B, 0)$, the predicted wave elevation based on the 'snap-shot' over a radial distance D and an angular separation $[\pi/2, 3\pi/2]$ can be expressed as,

$$\eta(r_B, 0; t+p) = \int_{R_A}^{R_B}\int_{\pi/2}^{3\pi/2} h_d(r_B-\rho, -\lambda)\eta(\rho,\lambda;t)d\lambda d\rho \tag{14}$$

Here $R_B = R_A + D$, where D is given by the first of equations (12). Once again, the point R_A may be chosen based on instrument range.

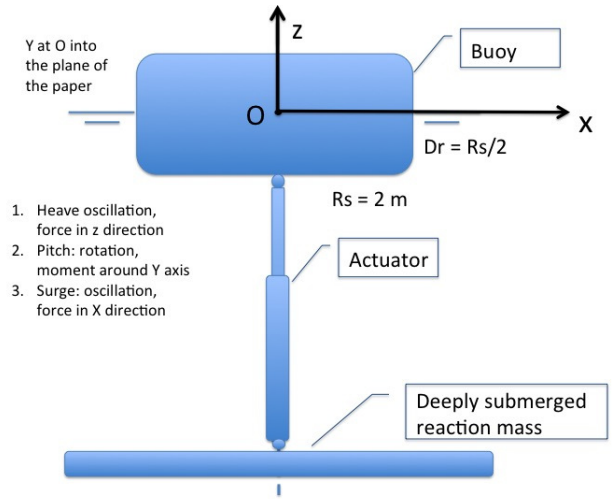

Fig. 3. A schematic view of the buoy discussed here. The reaction mass is assumed to be deeply submerged, and its own oscillations are neglected in what follows.

An illustration of the results for this approach is shown in section X. Here a bi-directional irregular wave field is assumed (this was generated using a Pierson-Moskowitz spectrum with a 'cosine-squared' angular spread. Additional directions add to the computational burden, and would require a more efficient computational implementation of the procedure than that used here.

V. Wave Energy Converter Studied

Figure 3 shows a schematic view of the wave energy converter used in the present simulations. A linear actuator is assumed to convert heave oscillations of a cylindrical buoy relative to a reaction mass that is submerged deep enough for its oscillations to be negligible in wave conditions of interest to power conversion. In the simulations performed here, the cylinder radius was assumed to be $R_s = 2$m, with its draft set at $D_r = 1$m.

$$[m + \overline{a}(\infty)]\dot{v}(t) + \int_0^\infty h_r(\tau)v(t-\tau)d\tau + c_d v(t) + k\int_{-\infty}^t v(\tau)d\tau = F_f(t) + F_L(t) \quad (15)$$

$$h_r(t) = \frac{2}{\pi}\int_0^\infty b(\omega)\cos\omega t d\omega = -\frac{2}{\pi}\int_0^\infty \omega a(\omega)\sin\omega t d\omega \quad (16)$$

$$a(\omega) = \overline{a}(\omega) - \overline{a}(\infty) \quad (17)$$

$\overline{a}(\omega)$, the frequency-dependent added mass in heave behaves as,

$$\lim_{\omega\to\infty}\overline{a}(\omega) \to \overline{a}(\infty) \quad (18)$$

$a(\omega)$ is thus the Fourier-transformable, frequency-variable part of $\overline{a}(\omega)$. Because $h_r(t)$ is real-valued and causal, $\omega a(\omega)$ and $b(\omega)$ are respectively, odd and even functions of frequency, and satisfy the Kramers-Kronig relations. Their full inverse Fourier transforms can be defined as,

$$h_a(t) = \frac{1}{2\pi}\int_{-\infty}^\infty \omega a(\omega)\mathrm{e}^{i\omega t}d\omega,$$
$$h_b(t) = \frac{1}{2\pi}\int_{-\infty}^\infty b(\omega)\mathrm{e}^{i\omega t}d\omega \quad (19)$$

Note that $h_a(t)$ is an odd function of t and $h_b(t)$ is an even function of t. Thus, $h_r(t) = h_a(t)+h_b((t)$ in the time domain, and hence, both h_a and h_b are non-causal. Therefore, their use in generating control forces on a wave-by-wave basis requires prediction of velocity v.

The exciting force $F_f(t)$, as commonly expressed in terms of the surface elevation at body centroid is,

$$F_f(t) = \int_{-\infty}^\infty h_f(\tau)\eta(x_B; t-\tau)d\tau \quad (20)$$

where τ is the integration variable. $\eta(x_B; t)$ is the wave surface elevation at buoy centroid x_B, and $h_f(t)$ is the impulse response function defining the exciting force in heave.

VI. Constrained Near-Optimal Wave-by-Wave Control

The goal of control is to drive the floating body at its hydrodynamic velocity optimum, subject to displacement and velocity constraints. This is accomplished by means of an actuation or control force that is evaluated in real time, using the predicted wave elevation and an impulse response function that is determined as described below. The buoy heave velocity $v(t)$ is hydrodynamically optimum (maximizing power transfer from the incident wave to the buoy), when $v(t) = v_o(t)$, where [18],

$$2c_d v_o(t) + 2\int_{-\infty}^\infty h_b(\tau)v_o(t-\tau)d\tau = F_f(t) \quad (21)$$

This condition can be achieved if the control force applied to the buoy is of the form [21],

$$F_L(t) = [m + \overline{a}(\infty)]\dot{v}_o(t) + k\int_{-\infty}^t v_o(\tau)d\tau + \int_{-\infty}^\infty h_a(\tau)v_o(t-\tau)d\tau - c_d v_o(t) - \int_{-\infty}^\infty h_b(\tau)v_o(t-\tau)d\tau \quad (22)$$

$F_L(t)$ can be seen to be a feedforward force, based on the desired velocity optimum $v_o(t)$. In practice, due to measurement errors and disturbances, a feedback loop will be required so that correct tracking is achieved. Measurement errors and disturbances are not accounted for in this paper.

F_L in equation (22) needs to be amended to reflect an oscillation constraint that requires the maximum excursion to be less than a specified limit, (e.g. the draft or the freeboard to avoid full emergence or full submergence). The frequency-domain approach of Evans [32] may be used as implemented in [21]. Briefly, this corresponds to using the non-causal

impulse response function h_{oc} to determine a constrained velocity v_{oc} instead of v_o in equation (22). Thus,

$$h_{oc}(t) = \frac{1}{2\pi}\int_{-\infty}^{\infty} \frac{H_f(i\omega)}{2[c_d + \Lambda(\omega) + b(\omega)]} \mathrm{e}^{i\omega t} d\omega \tag{23}$$

and,

$$v_{oc}(t) = \int_{-\infty}^{\infty} h_{oc}(\tau)\eta(x_B; t-\tau)d\tau \tag{24}$$

So that, the control force in the presence of a constraint is,

$$\begin{aligned} F_{Lc}(t) &= [m + \overline{a}(\infty)]\dot{v}_{oc}(t) + k\int_{-\infty}^{t} v_{oc}(\tau)d\tau \\ &+ \int_{-\infty}^{\infty} h_a(\tau)v_{oc}(t-\tau)d\tau - c_d v_{oc}(t) \\ &- \int_{-\infty}^{\infty} h_b(\tau)v_{oc}(t-\tau)d\tau \end{aligned} \tag{25}$$

The convolution integrals in equations (25) and (24) require foreknowledge of wave elevation at the device centroid x_B, which is provided by the deterministic wave prediction techniques discussed in sections II, and IV.

The captured power over a time duration T is given by,

$$P_{wr} = \frac{1}{T}\int_0^T F_{Lr}(t)v_{oc}(t)dt \tag{26}$$

where

$$F_{Lr}(t) = \int_{-\infty}^{\infty} h_b(\tau)v_{oc}(t-\tau)d\tau \tag{27}$$

The limits $\pm\infty$ in the integrals in equations (25) and (27) above are replaced by $-t_p$ and the present time t in practical simulations. Further, t_p is the prediction time defined such that $h_b(t) \to 0$ as $t \to -t_p$ [21].

With the average incident power over the buoy diameter $2R$ for an irregular wave quantified by a significant wave height H_s and an energy period T_e given by,

$$P_{inc} = 0.49 H_s^2 T_e (2R) \tag{28}$$

the capture width ratio (capture factor) can be found using

$$\eta_c = P_{wr}/P_{inc} \tag{29}$$

VII. Multi-resonant Control

Results are also obtained for a controller implementation that does not require up-wave measurements nor wave prediction. This approach is not designed to attempt to match the hydrodynamic velocity optimum in irregular waves, but rather, to generate the control force signal based on velocity or position feedback alone [33], [34]. Using on-line estimation of the frequency and amplitude/phase content in the feedback signal, reactive and resistive loads are computed for application by a linear actuator. Power electronics circuitry is used to set the actual force variation to be applied. The loads as computed are intended to provide resonance like behavior at 3 or more frequencies, in addition to the original natural frequency of the device.

VIII. Resistive Control

The control in this case simply consists of applying a damping load with the power take-off actuator. No wave prediction is required, but the damping level may be adjusted to match the 'internal' damping at the peak frequency of an incoming spectrum. No real-time feedforward or feedback forces are applied. Thus, the damping load D is set to

$$D = \alpha(b(\omega_p) + c_d) \tag{30}$$

α is set $\gg 1$, to keep the resistive force from being too small compared with the reactive forces in irregular waves for the small geometry being used here. In this case, the averaged captured power over a duration T is found using

$$P_{bl} = \frac{1}{T}\int_0^T D v_{bl}^2 dt \tag{31}$$

IX. Calculations and Simulations

For the geometry shown in Figure 3 (vertical cylinder radius $R = 2$m and draft $D_r = 1$m) simulations were carried out in a range of irregular wave conditions derived from the standard Pierson-Moskowitz type 2-parameter spectral representation, with a $\cos^2\theta$ directional spread. The spectra were represented using the expression,

$$S(\omega, \theta) = S(\omega)D_v(\theta) \tag{32}$$

where

$$\begin{aligned} S(\omega) &== \frac{131.5 H_s^2}{T_e^4 \omega^5} \exp\left[-\frac{1054}{(T_e\omega)^4}\right] \\ D_v(\theta) &= \frac{1}{2}\cos^2\theta \end{aligned} \tag{33}$$

The wave surface elevation at (x, t) can be expressed as

$$\begin{aligned} &\eta(x;t) = \\ &\sum_{n=1}^{N}\sum_{m=1}^{M} \Re\left\{A(\omega_n, \theta_m)\exp\left[-i\left(k(\omega_n)x - \omega_n t + \vartheta_n\right)\right]\right\} \end{aligned} \tag{34}$$

where,

$$A(\omega_n, \theta) = \sqrt{2S(\omega_n, \theta)\Delta\omega\Delta\theta} \tag{35}$$

and ϑ_n is a random phase angle $\in [0, 2\pi]$, with $S(\omega_n, \theta_m)$ representing the spectral density value at ω_n and direction θ_m. $N = 512$ was used in these calculations. Irregular wave records were computed for a range of spectra at significant wave height $H_s = 1$m, and energy periods T_e ranging from 7s to 17s. In order to minimize the computational burden (i.e. execution time), only a bi-directional spectrum is considered, although the current procedure is capable of functioning with multiple wave directions.

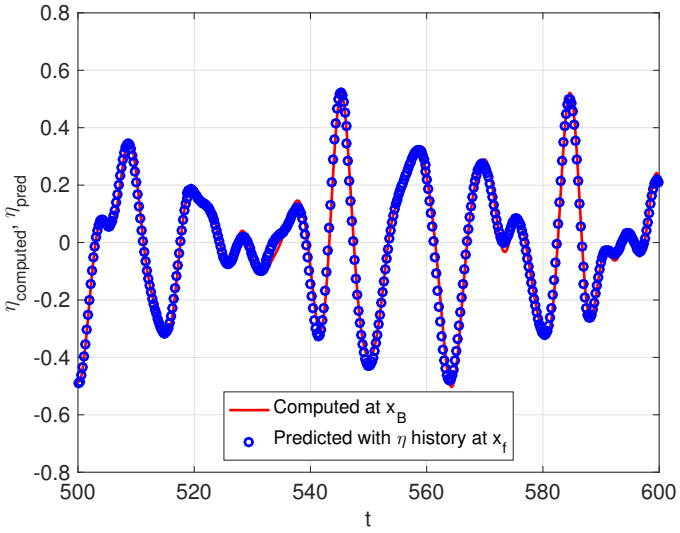

Fig. 4. A comparison between the predicted wave elevation at the device centroid using a 232s-long advancing wave elevation time series at a point 800m up-wave and the calculated wave elevation at the device centroid. The prediction time is 30s into the future. A long-crested wave field is assumed.

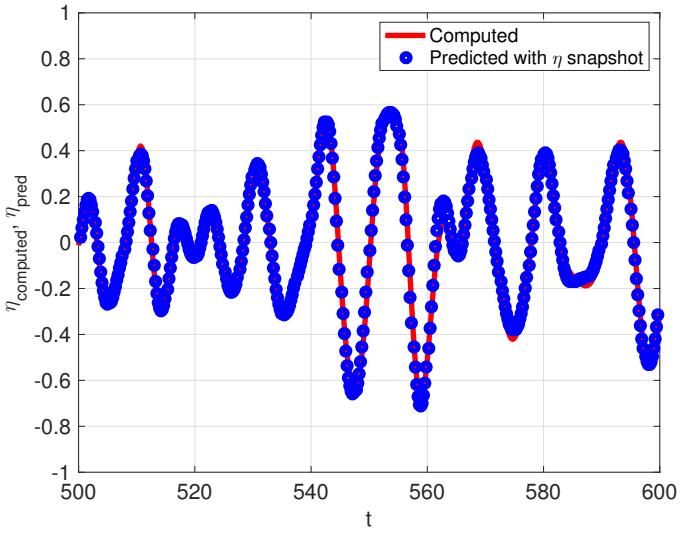

Fig. 5. A comparison between the predicted wave elevation at the device centroid using a fixed-time measurement approach. The length of the snap-shot is 800m. The prediction time is 30s into the future. A long-crested wave field is assumed.

X. Discussion of Results

Figure 4 shows a typical result for the fixed-point prediction approach in long-crested waves, for an irregular wave record for ($H_s = 1$m, $T_e = 11$s). A good match is seen between the predicted surface elevation time series and the actual, directly computed time series. Figure 5 plots the equivalent result using the fixed time technique for a long-crested irregular wave field. Again, good agreement is found between the predicted and the computed surface elevations. Our work so far [21], [35] has considered wave-by-wave control in long-crested waves. Here, simulation results are discussed for a wave-field with two predominant directions. Such wave fields frequently occur when swell and wind sea directions may be different at some sites (e.g. NDBC, Station 46006, Southeast Papa, April 16, 2017 [36]). Predictions were made at the device centroid about 30 s into the future, using a snapshot of the incoming wave field over about 800 m up-wave. The plot for a bi-directional wave field in Figure 6 shows a less-than-close match. Further work seems warranted in this case, though the source of the error appears to be more in the specific computer implementation than in the underlying analytical model.

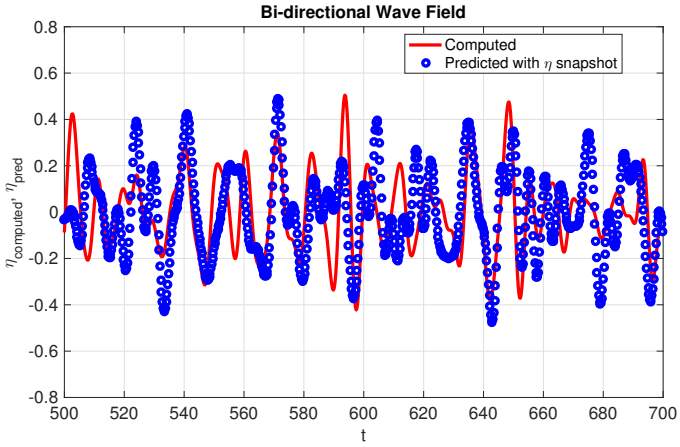

Fig. 6. A comparison between the predicted wave elevation at the device centroid using a fixed-time measurement approach. The radial length of the snap-shot is 800m. The prediction time is 30s into the future. A bi-directional wave field is assumed (with waves approaching from $\beta = 0$ degrees, and from $\beta = 40$ degrees).

Figures 7 and 8 plot the results for a situation when waves approach from two directions, as mentioned, at angles of incidence (1) 0 degrees, and (2) 45 degrees. For a range of energy periods T_e from 6s to 17s, the significant wave height H_s was again assumed to be 1m for these calculations. The predicted wave elevations shown in bi-directional wave fields using the present implementation were used in these calculations. For actuator efficiency of 85%, converted power (averaged over 10 minutes) under the wave-by-wave near-optimal control is found to be considerably greater than that available with baseline resistive control. The average conversion efficiency is seen to be greatest in the wave conditions dominated by shorter periods. This is likely the result of greater radiation damping at these periods for the present device, which enables greater power conversion within the swept-volume constraint. However, note that the incident wave power is greater for the longer-period dominated wave records, so the overall converted power is also greater despite the drop in efficiency. Figure 9 shows the maximum heave displacement observed over a 10-minute period. Overall, these results confirm that, if a prediction can be provided the required duration into the future, near-optimal control can be produced and performance improvement comparable to that observed in long-crested waves is possible [21]. It should be noted, however, that there has been an effort made here in the mechanical design to minimize the effect of surge and pitch modes. In the presence

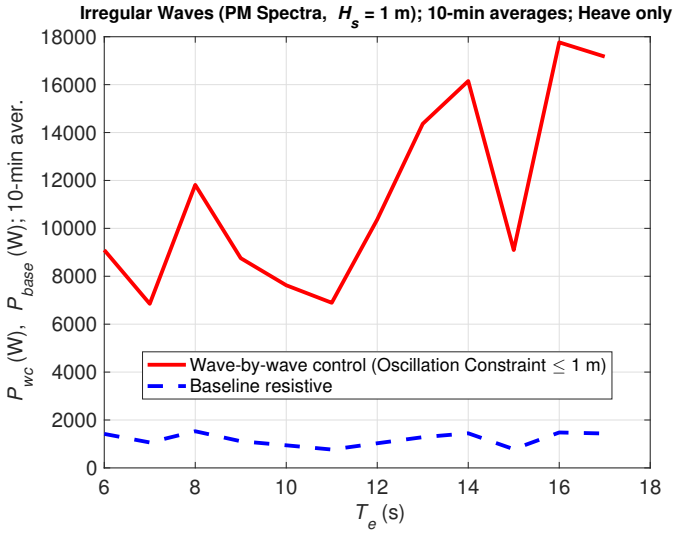

Fig. 7. Plot comparing the power absorbed with wave-by-wave impedance matching control (with baseline resistive control) in a bi-directional wave field containing waves approaching at incidence angles 0 deg and 45 deg. Displacement amplitudes were constrained to 1m for the buoy with radius 2m and draft 1m. Actuator efficiency was taken to be 85%. The 10-minute averages excluded the initial inactive periods during which the initial up-wave measurement time series were recorded.

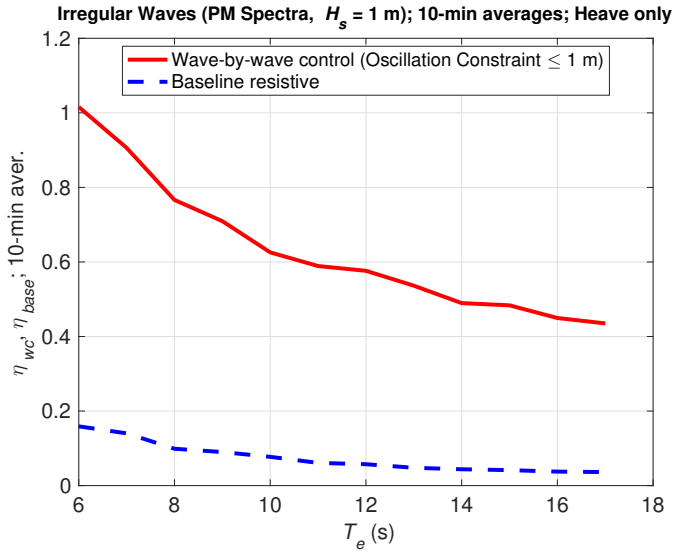

Fig. 8. Plot comparing the capture width ratio with wave-by-wave impedance matching control (with baseline resistive control) in a bi-directional wave field containing waves approaching at incidence angles 0 deg and 45 deg. Displacement amplitudes were constrained to 1m for the buoy with radius 2m and draft 1m. Actuator efficiency was taken to be 85%. The 10-minute averages excluded the initial inactive periods during which the initial up-wave measurement time series were recorded.

of the wave field from $\beta = 45$ degrees, sway and roll forcing will also exist. Actuator linkage design in practice will need to account for excitation in all 6 modes, while allowing buoy motion in heave alone, and will likely require some further research.

Figures 10 and 11 show results for the multi-resonant control algorithm. Note that, because this technique does not need wave measurement and prediction (but uses just the feedback of displacement or velocity), the control force is not directly dependent on wave direction. The plot in Figure 10 compares energy capture with the multi-resonant control (referred to as 'PDC3') with baseline resistive control. The plot in Figure 11 shows an overview result for the range of sea states examined for wave-by-wave control above. The control algorithm is seen to provide good energy capture with feedback alone.

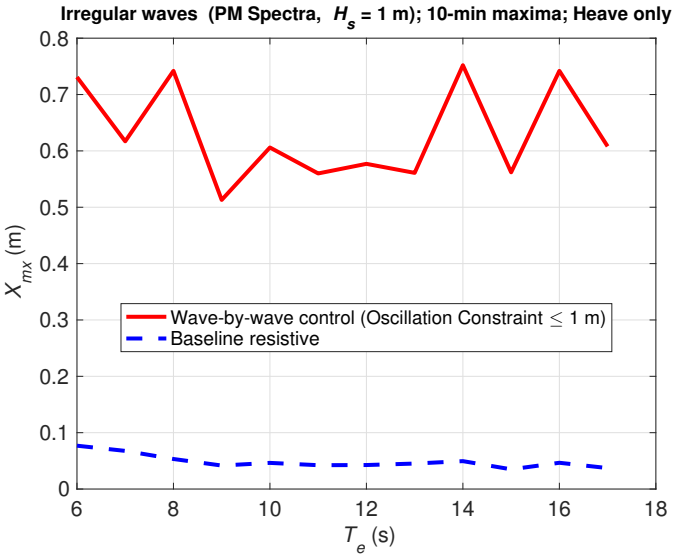

Fig. 9. Maximum oscillation amplitude under wave-by-wave impedance matching control (with baseline resistive control) in a bi-directional wave field containing waves approaching at incidence angles 0 deg and 45 deg. Displacement amplitudes were constrained to 1m for the buoy with radius 2m and draft 1m. Actuator efficiency was taken to be 85%. The 10-minute averages excluded the initial inactive periods during which the initial up-wave measurement time series were recorded.

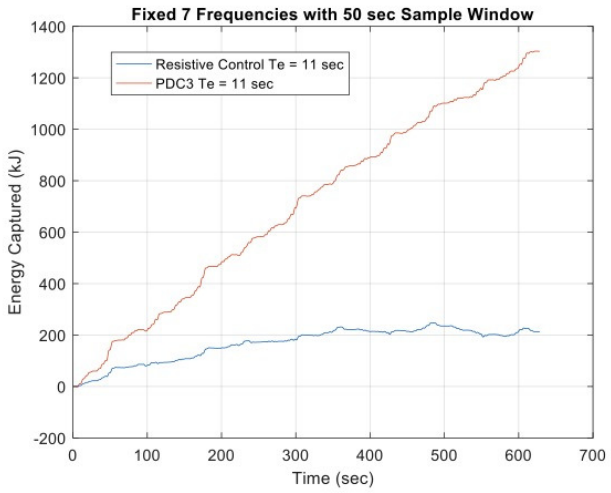

Fig. 10. Cumulative energy conversion for an irregular wave record with energy period = 11s, and significant wave height = 1m, with multi-resonant control. These results are for a full-scale cylinder buoy with radius =2m, and draft = 1m. Power conversion is through heave oscillations only, and displacement amplitudes are constrained to 1m.

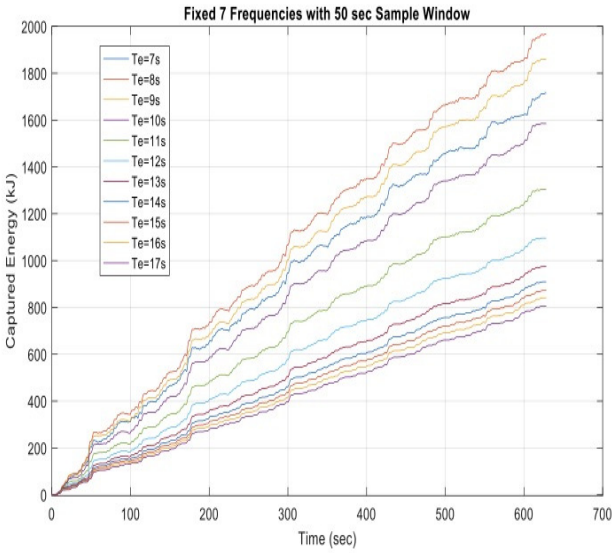

Fig. 11. Cumulative energy conversion for a range of wave spectra with multi-resonant control. The significant wave height in all cases is 1m. These results are for a full-scale cylinder buoy with radius =2m, and draft = 1m. Power conversion is through heave oscillations only, and displacement amplitudes are constrained to 1m.

XI. Conclusion

Two deterministic wave prediction techniques based on a linear wave propagation model were considered. Prediction distances and durations were on the order of 1000 meters and 30 seconds, respectively. Given the relative shortness of the prediction distance and time, effects of any wind forcing between the measurement point/region and the device were considered small enough to ignore. The propagation model was thus purely kinematic, based on the linear wave solution and the dispersion relation. A range of group velocities encompassing the propagation velocities of wave groups within practical wave spectra was considered for the so-called (i) fixed-point, and (ii) fixed-time techniques. For a bi-directional wave field, a heaving buoy type wave energy converter utilizing the prediction was used to provide an illustration of the improvement possible in the presence of prediction. While this control technique was based on 'feedforward' forcing, a feedback based multi-resonant controller was also considered for comparison. Overall, results show significant improvement in performance relative to purely resistive control, where no prediction is used and the damping level is adjusted using frequency-domain wave information.

Acknowledgements

We gratefully acknowledge the support of the US Defense Advanced Research Projects Agency (DARPA) under contract D16PC00143 and the support of the US National Science Foundation under grant 1635239. The views, opinions and/or findings expressed are those of the authors and should not be interpreted as representing the official views or policies of the Department of Defense or the National Science Foundation or the U.S. Government. Finally, we also wish to thank Professor R. C. Ertekin and Mr. Jiajun Song for providing the hydrodynamic results used in this work.

References

[1] A. F. O. Falcão, "Wave energy utilization: a review of the technologies," *Renewable and Sustainable Energy Reviews*, vol. 14, pp. 899–918, 2010.

[2] S. H. Salter, "Wave energy: nostalgic ramblings, future hopes, and heretical suggestions," *J. Ocean Engineering and Marine Energy*, vol. 2, no. 4, pp. 399–428, 2016.

[3] ——, "Development of the duck concept," in *Proc. Wave Energy Conference*, 1978, Heathrow, U.K.

[4] K. Budal and J. Falnes, "Optimum operation of improved wave power converter," *Marine Science Communication*, vol. 3, pp. 133–150, 1977.

[5] ——, "Interacting point absorbers with controlled motion," in *Power from Sea Waves*, B. Count, Ed. Academic Press, London, 1980, pp. 381–399.

[6] P. Nebel, "Maximizing the efficiency of wave-energy plants using complex conjugate control," *Proc. IMechE Part I - Journal of Systems and Control Engineering*, vol. 206, no. 4, pp. 225–236, 1992.

[7] D. Skyner, "Solo duck linear analysis," University of Edinburgh, Tech. Rep., 1987, technical Report.

[8] R. H. Hansen and M. M. Kramer, "Modeling and control of the wave star prototype," in *Proc. 9th European Wave and Tidal Energy Conference*, 2011, southampton, UK, paper 163.

[9] R. E. Hoskin, B. M. Count, N. K. Nichols, and D. A. C. Nicol, "Phase control for the oscillating water column," in *Proc. IUTAM Symp. Hydrodynamics of Wave Energy Utilization*, D. V. Evans and A. F. de O. Falcão, Eds. Springer Verlag, Berlin, 1985, pp. 257–268.

[10] J. N. B. A. Perdigao and A. J. N. A. Sarmento, "A phase control strategy for OWC devices in irregular waves," in *Proc. 4th Int. Workshop on Water Waves and Floating Bodies*, J. Grue, Ed., 1989, pp. 205–209.

[11] A. F. O. Falcão and P. A. P. Justino, "OWC wave energy devices with air flow control," *Ocean Engineering*, pp. 1275–1295, 1999.

[12] A. F. O. Falcão, "Phase control through load control of oscillating body wave energy converters with hydraulic PTO system," *Ocean Engineering*, vol. 35, pp. 358–366, 2008.

[13] U. A. Korde, "Phase control of floating bodies from an on-board reference," *Applied Ocean Research*, vol. 23, pp. 251–262, 2001.

[14] A. Babarit and A. H. Clement, "Optimal latching control of a wave energy device in regular and irregular waves," *Applied Ocean Research*, vol. 28, no. 2, pp. 77–91, 2006.

[15] S. Salter, J. Taylor, and N. Caldwell, "Power conversion mechanisms for wave energy," *Proc. Institution of Mecahnical Engineers, Part M–Journal of Engineering for the Maritime Environment*, vol. 216, pp. 1–27, 2002.

[16] A. Babarit, M. Guglielmi, and A. Clement, "Declutching control of a wave energy converter," *Ocean Engineering*, vol. 36, pp. 1015–1024, 2009.

[17] S. Naito and S. Nakamura, "Wave energy absorption in irregular waves by feedforward control system," in *Proc. IUTAM Symp. Hydrodynamics of Wave Energy Utilization*, D. Evans and A. de O. Falcão, Eds. Springer Verlag, Berlin, 1985, pp. 269–280.

[18] J. Falnes, "On non-causal impulse response functions related to propagating water waves," *Applied Ocean Research*, vol. 17, no. 6, pp. 379–389, 1995.

[19] J. L. Forsberg, "On-line identification and prediction of incident waves," in *Proc. IUTAM Symp. Hydrodynamics of Wave Energy Utilization*, D. Evans and A. de O. Falcão, Eds. Springer Verlag, Berlin, 1985, pp. 185–193.

[20] M. R. Belmont, J. M. K. Horwood, R. W. F. Thurley, and J. Baker, "Filters for linear sea-wave prediction," *Ocean Engineering*, vol. 33, no. 17–18, pp. 2332–2351, 2006.

[21] U. A. Korde and R. C. Ertekin, "Wave energy conversion by controlled floating and submerged cylindrical buoys," *Journal of Ocean Engineering and Marine Energy*, vol. 1, no. 3, pp. 255–272, 2015.

[22] F. Fusco and J. Ringwood, "Short-term wave forecasting for real-time control of wave energy converters," *IEEE Trans. on Sustainable Energy*, vol. 1, no. 2, pp. 99–106, 2010.

[23] F. Paparella, K. Monk, V. Winands, M. Lopes, D. Conley, and J. V. Ringwood, "Up-wave and autoregressive methods for short-term wave forecasting for an oscillating water column," *IEEE Transactions on Sustainable Energy*, vol. 6, no. 1, pp. 171–178, 2015.

[24] M. P. Schoen, J. Hals, and T. Moan, "Wave prediction and robust control of heaving wave energy devices for irregular waves," *IEEE Trans. Energy Conversion*, vol. 26, no. 2, pp. 627–638, 2011.
[25] F. Fusco and J. V. Ringwood, "A study of the prediction requirements in real-time control of wave energy converters," *IEEE Transactions on Sustainable Energy*, vol. 3, no. 1, pp. 176–184, 2012.
[26] G. Wu, "Direct simulation and deterministic prediction of large-scale nonlinear wave field," Ph.D. dissertation, Massachusetts Institute of Technology, 2004, cambridge, MA.
[27] J. Dannenberg, P. Naaijen, K. Hessner, H. den Boom, and K. Reichert, "The on board wave and motion estimator OWME," in *Proc. Int. Soc. Offshore and Polar Engr. Conf.*, 2010, beijing, China.
[28] B. Lund, C. O. C. III, H. Tamura, and H. C. Graber, "Multi-directional wave spectra from marine x-band radar," *Ocean Dynamics*, June 2016.
[29] J. N. Newman, *Marine Hydrodynamics*. Cambridge: MIT Press, 1978, second Printing, Call No. (VM 156.N48)., ix + 402 pp.
[30] M. Schetzen, *The Volterra and Wiener Theories of Nonlinear Systems*. John Wiley & Sons, NY, 1980, a Wiley-Interscience publication.
[31] U. A. Korde, "Hydrodynamic modeling and control of buoy oscillations for efficient conversion of wave power in ocean sensing," in *Proc. ONR/MTS Buoy Workshop 2016*, April 2016, woods Hole, MA.
[32] D. V. Evans, "Power from water waves," *Annual Review of Fluid Mechanics*, vol. 13, pp. 157–187, 1981.
[33] D. G. Wilson and R. D. R. III, "PD version of complex-conjugate controller for optimal wec performance," Sandia National Laboratories, Tech. Rep., March 2015, sD # 13535.
[34] J. Song, O. O. Abdelkhalik, R. D. Robinett, G. Bacelli, D. G. Wilson, and U. A. Korde, "Multi-resonant feedback control of heave wave energy converters," *Ocean Engineering*, vol. 127, pp. 269–278, 2016.
[35] U. A. Korde, R. D. Robinett, and D. G. Wilson, "Wave-by-wave control in irregular waves for a wave energy device with approximate parameters," *J. Ocean Engineering and Marine Energy*, vol. 2, no. 4, pp. 509–519, 2016.
[36] NDBC, "Station 46006: Southeast Papa," 2017, http://www.ndbc.noaa.gov, April 16, 2017.